AGU PUBLICATIONS

Geochemistry, Geophysics, Geosystems

RESEARCH ARTICLE
10.1002/2015GC006102

Special Section:
The Lithosphere-asthenosphere System

Questions on the existence, persistence, and mechanical effects of a very small melt fraction in the asthenosphere

Benjamin K. Holtzman[1]

[1]Lamont Doherty Earth Observatory, Columbia University, Palisades, New York, USA

Abstract This paper integrates current questions in rock physics on the effects and behavior of very small melt fractions ($\ll$ 1%) in the asthenosphere. In experiment and theory, it has been shown that a very small melt fraction forming a connected network has a large effect on the diffusion creep shear viscosity, as well as in the anelastic behavior. Because small concentrations of volatiles, particularly H_2O and CO_2, significantly lower the peridotite solidus, a small melt fraction is expected in the asthenosphere. Even with connected networks, permeability will be low and surface tension will generate a strong force resisting complete draining of small melt fractions. The anelastic reduction of shear velocity due to melt could cause a $\geq$ 5% shear velocity contrast across the solidus, consistent with the contrast measured on features in the shallow suboceanic upper mantle that are often interpreted as the lithosphere-asthenosphere boundary.

Key Points:
- A very small melt fraction in a network has a dramatic effect on the diffusion creep viscosity
- This melt is stabilized by volatiles and surface tension will prevent it from being drained
- The effect of melt on anelastic behavior can explain seismic structure in the shallow upper mantle

Correspondence to:
B. K. Holtzman,
benh@ldeo.columbia.edu

Citation:
Holtzman, B. K. (2016), Questions on the existence, persistence, and mechanical effects of a very small melt fraction in the asthenosphere, *Geochem. Geophys. Geosyst.*, *17*, 470–484, doi:10.1002/2015GC006102.

Received 16 SEP 2015
Accepted 4 DEC 2015
Accepted article online 14 DEC 2015
Published online 17 FEB 2016
Corrected 12 MAR 2016

This article was corrected on 12 MAR 2016. See the end of the full text for details.

1. Introduction

The shallow upper mantle may be characterized by regions of relatively high and low strain rates and melt productivity. Plumes, mid-ocean ridges, subduction zones, and small-scale convection constitute the former, while relatively stationary regions of suboceanic mantle constitute the latter, as illustrated in Figure 1a. This paper emphasizes the latter regions of the upper mantle, in which there may be small volumes of melt present that are thermodynamically and mechanically stable, and significantly affect mechanical properties. To first order, the thermal structure of the upper mantle determines the mechanical structure of the plates. However, it not well understood yet to what extent the suboceanic low-velocity zone (LVZ) is determined by temperature, melt and/or volatile content, and to what extent the low velocity corresponds to low viscosity. Similarly, how strong and spatially varying is the contrast in mechanical properties across the lithosphere-asthenosphere boundary (LAB)? What thermal and compositional gradients determine the properties of this interface?

The idea that partial melt explained the seismic low-velocity zone beneath oceanic lithosphere took hold in the 1970s [e.g., *Anderson and Sammis*, 1970], along with experimental studies showing that volatiles (especially H_2O and CO_2) enable the asthenosphere to be partially molten [e.g., *Green and Liebermann*, 1976; *Eggler*, 1976]. Subsequently, upon recognizing the profound effects of dissolved water in the olivine lattice on its mechanical properties, people have considered the idea of a subsolidus asthenosphere [e.g., *Hirth and Kohlstedt*, 1996; *Karato and Jung*, 1998; *Karato*, 2012]. In this scenario, the oceanic plates form at depths below the mid-ocean ridge where the dry solidus is crossed and large-volume silicate melting leaves olivine dry and stronger. This process and effect may well occur and influence the strength of plates by dehydration at the mid-ocean ridge [e.g., *Hirth and Kohlstedt*, 1996; *Phipps Morgan*, 1997; *Braun et al.*, 2000; *Karato*, 2012].

However, in the last decade, ideas have emerged that complicate the extrapolation and interpretation of the role of water in the upper mantle. Improvements in experimental methods and understanding have further demonstrated that the upper mantle can be effectively fluxed by small concentrations of volatiles, primarily H_2O and CO_2 [e.g., *Dasgupta et al.*, 2007; *Hirschmann*, 2010]. Thus, where there are volatiles in the mantle above the water-depressed solidus, there is likely to be melting (and melt). Because CO_2 does not partition into the solid and is also effective at lowering the solidus, melt present in the asthenosphere may grade from basaltic to carbonatitic in composition [e.g., *Dasgupta et al.*, 2007; *Hirschmann*, 2010]. In parallel, new measurements of the electrical conductivity of the suboceanic upper mantle suggested the presence of CO_2-rich melts [e.g., *Gaillard et al.*, 2008]. These conductivity measurements and experimental observations support the idea

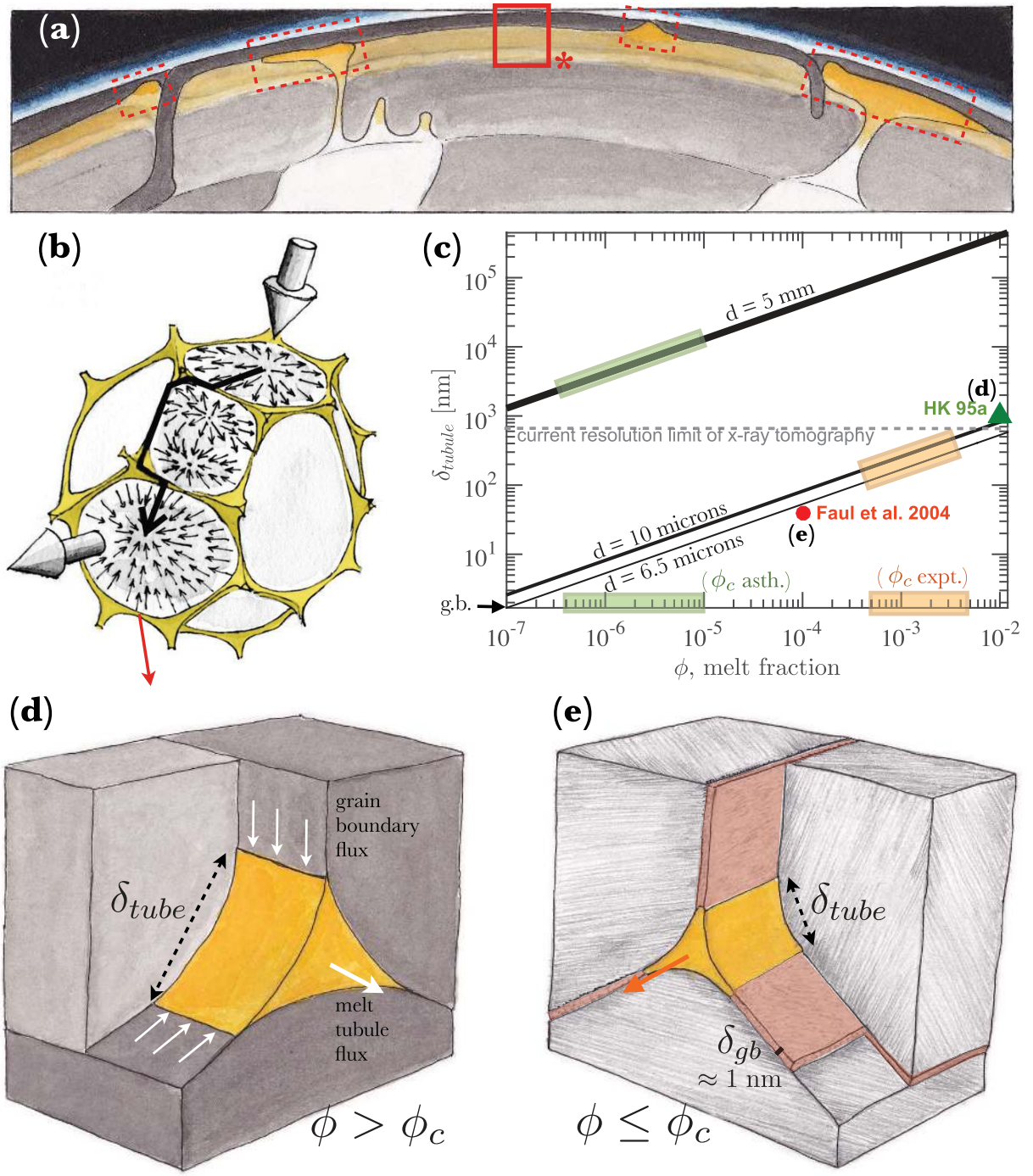

Figure 1. What is a very small melt fraction? (a) Upper mantle dynamics, roughly to scale. Yellow indicates possible partially molten regions. Red dashed squares indicate high strain rate, high productivity regions. Solid square indicates potentially low productivity and lower strain rate regions that may contain very small melt fractions. (b) Illustration of the contiguity model for grain boundary diffusion creep. At very small ϕ, connected networks can form and drastically reduce diffusion distances across grain faces, causing significant weakening simply by a 3-D geometric effect. ϕ_c is the critical melt fraction above which the matter flux through the melt network no longer limits creep rate—only the diffusion through grain boundaries does. (c) Melt tubule length scale, δ_{tubule}, as a function of melt fraction for different grain sizes, and two experimental data points, discussed in the text. Estimates of ϕ_c and corresponding δ_{tubule} values are shown for experimental and natural grain sizes, calculated in section 2.5. (d) A typical triple junction melt tubule, much thicker than the grain boundary. (e) For $\phi \leq \phi_c$, the tubule dimension can approach the grain boundary thickness (by a factor of about 10 here, for illustration).

that there are small degrees of melt produced everywhere in the shallow upper mantle, at temperatures above the volatile-fluxed solidus. Thus, debate continues on the thermodynamic origin of the asthenosphere and the relative contributions of H_2O, CO_2, and melt.

In the following, I synthesize results from experiments and theory demonstrating that very small, connected melt fractions have a significant effect on the mechanical properties of rocks at high temperature (section 2). I will then argue the asthenosphere always maintains (at least) a very small amount of melt, rendered unextractable by surface tension (section 3), which significantly affects the mechanical properties and thus our interpretation of seismic velocity measurements (section 4).

2. What is the Effect of Melt on Viscosity?

In 2009, Takei and Holtzman developed a new constitutive model for grain boundary diffusion (Coble) creep of partially molten rocks [*Takei and Holtzman*, 2009a, 2009b, 2009c, hereinafter TH1,2,3]. One of the principal findings of this model, elucidated in TH1 and TH2, was the rapid enhancement of strain rate from zero to very small melt fractions upon the development of a connected network of melt tubules, which implies that the onset of melting brings significant effects on shear and bulk viscosity. This prediction is consistent with experimental measurements of shear viscosity (the focus of this paper) in partially molten rock analog [*McCarthy and Takei*, 2011], synthetic olivine [*Faul and Jackson*, 2007], and San Carlos olivine [e.g., *Hirth and Kohlstedt*, 1995a; *Mei et al*., 2002], discussed further below.

2.1. What is a "Very Small" Melt Fraction?

The cause of this increase in strain rate is the sharp reduction of diffusion distance upon formation of a connected melt network, even with a very small melt volume fraction, ϕ. Network formation is expected for melt-rock systems with a dihedral angle of $\theta < 60^\circ$ [*Wark and Watson*, 2000], such as basalt-peridotite ($10^\circ < \theta < 35^\circ$) [e.g., *von Bargen and Waff*, 1986; *Cooper and Kohlstedt*, 1986; *Garapić et al*., 2013], and carbonatite-peridotite ($\theta < 30^\circ$) [e.g., *Minarik and Watson*, 1995], as illustrated in Figure 1b. *Minarik and Watson* [1995] demonstrate that carbonatite melt connectivity exists down to $\phi \approx 0.0001$ in experiments, and to much smaller melt fractions for mantle grain sizes. *Faul et al*. [2004] and *Garapić et al*. [2013] observe triple junction tubules with diameters on the order of tens of nanometers, corresponding to a melt fraction of ϕ=0.0001 at a mean grain size d=6.5 μm, plotted in Figure 1c. An approximation of the length scale of a triple junction tubule wall, δ_{tube}, as a function of melt fraction is derived in Appendix A and is consistent with these measurements. As illustrated in Figures 1d and 1e, δ_{tube} values for very small melt fractions are still significantly larger than the thickness of a typical grain boundary $\delta_{g.b.}$, of 1 nm [e.g., *Hiraga et al*., 2007]. However, these tubules are well below the resolution of current X-ray tomography of $\approx 0.7\ \mu$m, as utilized to image connectivity in experimental samples as in *Zhu et al*. [2011] and *Miller et al*. [2014]. As shown in Figure 1c, even very small melt fractions ($\phi \ll 0.01$) provide enough melt mass for surface tension to organize melt into connected networks of triple junction tubules. It is the existence, effects and persistence of these networks of very small tubules that is of interest here.

2.2. Synthesis of Experimental and Theoretical Results

It has recently become possible to measure effects of such small melt fractions on the shear viscosity, by fabricating very pure materials and then doping them with melt compositions, as in *Faul and Jackson* [2007] for olivine and *McCarthy and Takei* [2011] for analog materials. *Faul and Jackson* [2007] found a reduction by a factor of about 20 (defined as x_{ϕ_c} below), with $\phi \approx 0.0002$ in sol-gel + basalt samples, as illustrated in Figure 2. In experiments on the silicate rock analog borneol, *McCarthy and Takei* [2011] could isolate a chemical effect by comparing pure borneol to a binary eutectic mixture of borneol-diphenylamine. They measured viscosity and attenuation above and below the solidus. For the effect of melt on viscosity, they measured a total x_{ϕ_c}=40. The interpretation of the origin of this weakening effect is discussed below in section 2.4.

How can one predict the mechanical effects of such small melt fractions? "Contiguity" is a state variable well-suited to describing the effects of melt on mechanical properties, defined as the ratio of grain surface area in contact with neighboring grains to the total grain surface area [*Takei*, 1998]. The "contiguity model" as written in TH1,2,3 describes a situation in which chemical disequilibrium between melt and solid exists due to an applied stress (i.e., the local chemical potential, $\mu_i \propto \sigma_n \Omega_i$, where σ_n is the normal stress and Ω is the partial molar volume of component i). The gradient in normal stress (or local traction) around a grain drives diffusion of matter from grain faces under relative compression to those under relative tension, and the rate of change (and thus the macroscopic viscosity) depends on the kinetics of matter transport [*Lehner*, 1995; *Takei and Holtzman*, 2009a]. As illustrated in Figure 1b (and in Figure 5 of TH1), a connected melt

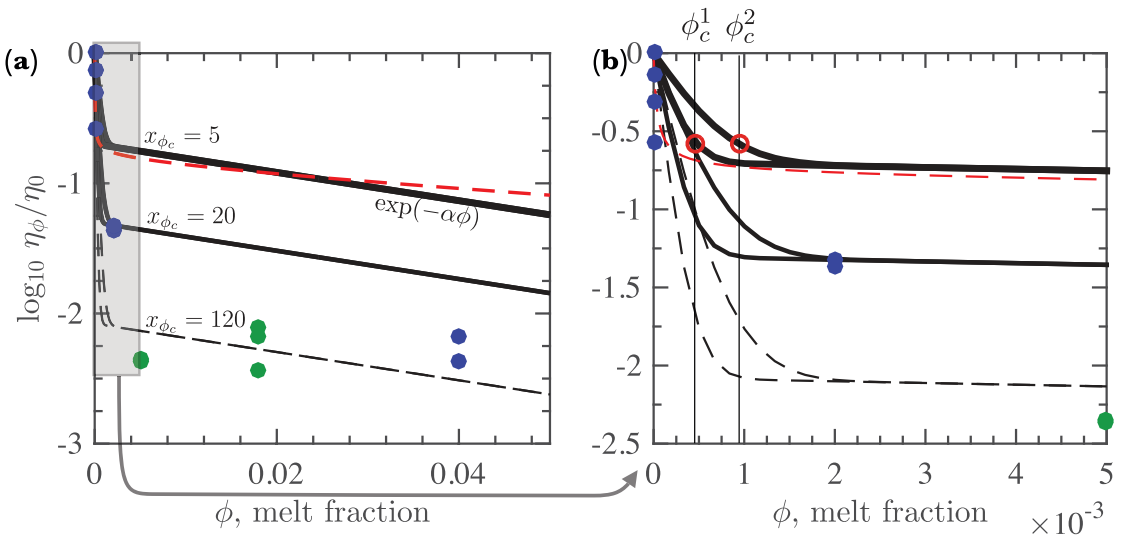

Figure 2. (a) Four curves of the parameterization, for values $\phi_c = 0.0005$ *and* $\phi_c = 0.001$, $x_{\phi_c} = 5,\ 20,\ 120$. The red dashed line shows a full calculation from TH2. (b) A zoom in on low melt fraction. Green dots are data from *Hirth and Kohlstedt* [1995a, 1995b]; blue dots indicate *Faul and Jackson* [2007] data, discussed in sections 2.2, 2.4, and Appendix C.

network dramatically reduces the *effective* diffusion distance between those faces. In the 3-D version of the model, TH1 assumed infinitely fast diffusivity in the melt, which lead to a step function reduction in viscosity at zero melt fraction, with a reduction factor of $x_{\phi_c} = 5$, using a 14-face (tetrakaidekahedral) geometry of contact patches. In TH2, the singularity is removed by analyzing the diffusive fluxes at small melt fractions with finite melt diffusivity; the definition of a critical melt fraction, ϕ_c, is associated with the completion of this rapid reduction in viscosity, as illustrated in Figures 1 and 2. For $0 < \phi < \phi_c$, viscosity is strongly sensitive to melt fraction; for $\phi_c < \phi < \phi_{disagg.}$, the sensitivity is more moderate, discussed below, where $\phi_{disagg.}$ is the melt fraction (range) at which the solid disaggregates [e.g., *Scott and Kohlstedt*, 2006; *Renner et al*., 2000]. As developed below in section 2.5, ϕ_c should be on the order of 10^{-3} for experimental grain sizes and $10^{-5} - 10^{-6}$ for natural grain sizes.

2.3. A New Parameterization for the Melt Effect on Viscosity

I provide a new parameterization of the effect of melt on shear viscosity that incorporates the effect of very small melt fractions. This function may be of value to experimentalists in analysis of data and others in exploring potential geodynamical consequences of this rheological behavior. It captures the behavior of the contiguity model, with two parameters to describe the effects of $\phi \leq \phi_c$:

$$\dot{\varepsilon}'_\phi = \frac{\dot{\varepsilon}_\phi}{\dot{\varepsilon}_0} = e^{(\alpha\phi + c_1 \mathrm{erf}(c_2\phi))}, \tag{1}$$

where α is the well-known empirically determined constant, ~26 for diffusion creep in olivine-basalt systems [*Mei et al*., 2002]. c_1 is a factor describing the magnitude of the increase in strain rate at ϕ_c, as $c_1 = \ln(x_{\phi_c})$, where x_{ϕ_c} is the strain rate amplification factor (or viscosity reduction factor) at ϕ_c. The second factor, c_2, describes the rate of reduction with melt fraction, and is related to ϕ_c as $c_2 \approx 1/\phi_c$, such that the error function term can be written as $c_1 \mathrm{erf}(\phi/\phi_c)$. Alternatively, one can use this function directly on the viscosity, as $\eta'_\phi = \frac{\eta_\phi}{\eta_0} = e^{-(\alpha\phi + c_1 \mathrm{erf}(\phi/\phi_c))}$. In Figures 2a and 2b, examples of the parameterization are shown, fitting experimental data discussed below. For $\phi = 0 - 0.04$, the parameterization closely fits the results of the full calculation from TH2, shown by the red dashed line. Above about $\phi = 0.10 - 0.15$ (not shown in Figure 2), the parameterization diverges from the model [*Takei and Holtzman*, 2009a, Figure 11b]. In the following, I discuss current questions on the physics affecting the values of the fitting parameters.

2.4. What Is the Magnitude of Strain Rate Enhancement?

In experimental studies, it is difficult but possible to separate the "geometric" effects described by the contiguity model ($x_{\phi_c} = 5$) from additional "chemical" effects on the diffusion kinetics in the melt, lattice, and grain

boundaries. *McCarthy and Takei* [2011] propose that the geometric and chemical effects are multiplicative, i.e., $x_{\phi_c} = x^g_{\phi_c} x^c_{\phi_c}$. Impurities and defects affect the relative diffusivities in the melt, lattice, and grain boundaries. It is known that grain boundaries incorporate a higher concentration of trace and incompatible elements than do lattices [e.g., *Hiraga and Kohlstedt*, 2007; *Hiraga et al.*, 2007], increasing the grain boundary diffusivity with increasing impurity content. Dissociated water (i.e., $H^+ + OH^-$) may also concentrate along the grain boundary [*Hiraga et al.*, 2007]. The relative degrees of water and other defect-induced enhancement of diffusion in the melt, grain boundary, and lattice will determine the chemical effects ($x^c_{\phi_c}$), but are incompletely understood.

As observed in *Faul and Jackson* [2007], a viscosity reduction of about a factor of $x_{\phi_c} \approx 20$ occurs with $\phi \approx 0.0002$. The addition of basalt powder introduces chemical components that are not present in the truly melt-free sol-gel material. Thus, as the basalt equilibrates with the sol-gel matrix, the chemical effects (including enhancement of lattice and grain boundary diffusivities) would contribute approximately a factor of 4, if the geometric effect contributes a factor of 5 as predicted. In samples with $\phi = 0.04$, the samples are significantly weaker than $x_{\phi_c} = 20$, suggesting that chemical effects continue to be enhanced on the sol-gel samples. *McCarthy and Takei* [2011] could isolate a chemical effect by comparing pure borneol to a binary mixture of borneol-diphenylamine, which produces a eutectic melt, analogous to the *Faul and Jackson* [2007] experiments. For the effect of melt on viscosity, they measured a total $x_{\phi_c} = 40$. The subsolidus effect of the added components on shear viscosity was measured by comparing the data from pure borneol to that of the eutectic mixture, which yielded a weakening factor of 8. This factor was interpreted as an estimate of the chemical effect, $x^c_{\phi_c}$, leading to a constraint on the geometric effect: $x^g_{\phi_c} = 40/8 = 5$, consistent with the model prediction. The systematic dependences of the geometric and chemical effects on T, P, major and trace element compositions constitute open questions.

Experiments on samples derived from San Carlos (or other) mantle xenoliths [e.g., *Hirth and Kohlstedt*, 1995a, 1995b, 2003; *Mei et al.*, 2002; *Zimmerman and Kohlstedt*, 2004; *Hansen et al.*, 2011] do not show the sudden weakening above $\phi = 0$, but are far weaker than the sol-gel samples (except for the $\phi = 0.04$ sample). As illustrated in Figure 2, the data from both sources are compared by selecting low stress-, high T samples from the diffusion creep field from *Hirth and Kohlstedt* [1995a] and then scaling strain rates by grain size, temperature, and stress, described in Appendix C1; $x_{\phi_c} \approx 120$ relative to the sol-gel samples. The San Carlos and other naturally derived samples are prepared by pulverizing and density-separating the powders to remove other phases, but the process is imperfect, so these experiments are referred to in the literature as "nominally melt-free." One way to explain the lack of rapid weakening at small melt fractions is that samples of reconstituted natural materials always contain small amounts of phases that melt at the conditions of creep experiments. If this nominal melt fraction is at or above the critical melt fraction (as it appears to be in Figure 1c), the difference between sol-gel and naturally-derived samples could be reduced by at least $x^g_{\phi_c}$. If so, these natural material-based flow laws [e.g., *Hirth and Kohlstedt*, 2003; *Mei et al.*, 2002; *Zimmerman and Kohlstedt*, 2004; *Hansen et al.*, 2011] are applicable directly to regions of the mantle above a solidus, but diffusion creep viscosity estimates for sub-solidus regions must be increased by $x^g_{\phi_c}$. (Other deformation mechanisms are affected differently by melt, discussed further in Section 4.1 and Appendix C1.). The differences between sol-gel and naturally derived olivine samples need to be better understood through experiments and theory.

2.5. How Does ϕ_c Depend on Grain Size?

TH2 demonstrated that ϕ_c should depend on grain size, d. The onset of the weakening effect of melt depends on the resistance to flux through the network of tubules, which depends on the diffusivity of matter into and through the network. Because the melt geometry is self-similar with respect to grain size, in a representative volume, there will simply be more length of tubules of the critical cross-sectional area in a fine-grained rock than in a coarse-grained one, such that ϕ_c increases with decreasing grain size, as discussed further in Appendix A. More quantitatively, TH2 defined three dimensionless scaling parameters, α, β, and γ, that characterize the various contributions to the total diffusive flux through melt during deformation, cast in terms of resistance to diffusion. γ describes the resistance to matter diffusion through the melt network, relative to the resistance to diffusion through the grain boundaries, in their equation (37), as

$$\gamma = \left[\frac{S^{GB}}{S^L}\right]\left[\frac{D^{GB}}{D^L}\right]\left[\frac{3\pi}{4}\frac{da}{dC}\bigg|_{C_0}\frac{(1-C_0)}{a_0}\right], \tag{2}$$

where C is the concentration of the creep rate-limiting component in the melt (i.e., a pure solid of component A and a binary liquid of components A and B), and a is the activity of that creep-rate-limiting

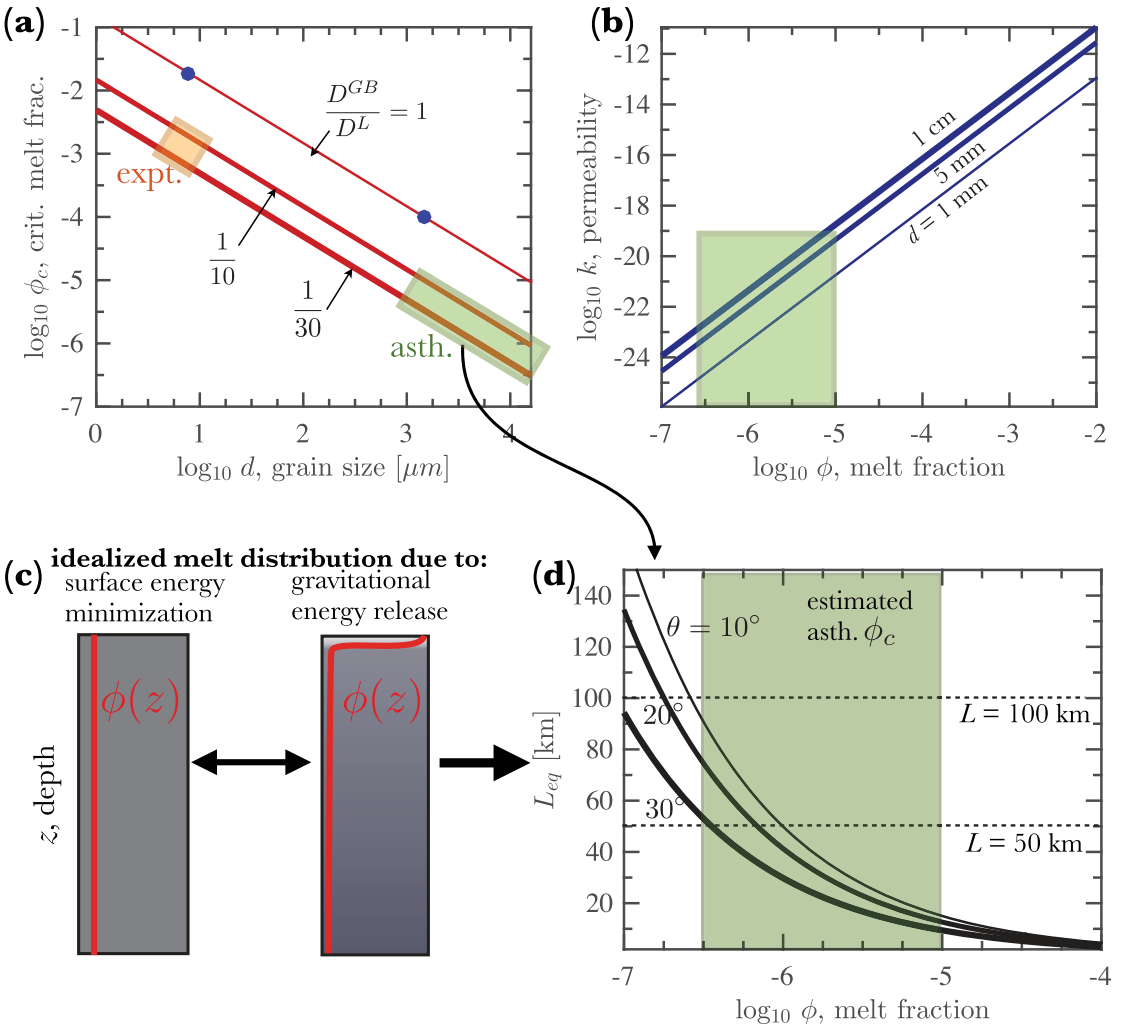

Figure 3. (a) Critical melt fraction as a function of grain size, for three values of $\frac{D^{GB}}{D^L}$ (1.0, 0.1, 0.033). Blue dots indicate the solutions in TH2. Orange and green boxes indicate estimates for experimental and asthenospheric grain sizes. (b) Permeability as a function of melt fraction, for d = 1, 5, 10 mm. (c) Cartoon illustrating the competition between interfacial and gravitational potential energy. (d) $L_{eq.}$, the length scale at which these energies are equivalent, as a function of ϕ, parameterized by θ. The rapid increase with decreasing ϕ indicated that it becomes increasingly difficult for gravity to drain a region as melt fraction decreases.

component A. S^{GB} and S^L are the cross-sectional areas through which the flux occurs from grain boundaries and melt phase, respectively (see Figure 3 of TH2), D^{GB} and D^L are the diffusivities of component A in the grain boundary and melt. This equation can be simplified as follows, as discussed in paragraph 35 of TH2: (1) assuming near ideality, the term $\frac{da}{dC}|_{C_0} \frac{(1-C_0)}{a_0} \approx 1$ and (2) the ratio simplifies to $\left[\frac{S^{GB}}{S^L}\right] = \frac{2.5}{\phi}\frac{\delta}{R}$, where δ is the thickness of the grain boundary and R is the grain radius. Furthermore, they chose a critical value of γ (γ_c=0.02) that corresponds to the onset of the rapid decrease in grain boundary flux as contiguity $\varphi \rightarrow 1$, as a way to identify ϕ_c.

Here I further simplify equation (2), using γ_c=0.02 in equation (2) and rearranging for ϕ_c,

$$\phi_c(d) = \frac{B}{\gamma_c}\frac{D^{GB}}{D^L}\frac{\delta}{d}, \tag{3}$$

where B=3.75π and the grain size d=2R. This equation illustrates important aspects of the proposed physics: (1) $\phi_c \propto d^{-1}$ and (2) ϕ_c is sensitive to ratio of D^{GB} and D^L, as shown in Figure 1d, both of which are not well known (TH2), discussed in section 2.2. Estimates of the ratio D^{GB}/D^L come from Appendix B1 of TH2, using equations (36) (2-D) and 44 (3-D) of TH1. However, an omission was made in TH2, of the factor 1/16 (2-D) and 1/30 (3-D) in calculating D^{GB} (Y. Takei, personal communication, 2015). As a result, D^{GB}/D^L

was overestimated in TH2. In Figure 3a, I plot original and corrected solutions for $\frac{D^{GB}}{D^{L}} = 1, 1/10, 1/30$. The blue dots show the solutions shown in TH2. The corrected solutions show that $\phi_c = 5\times10^{-4} - 5\times10^{-3}$ for experimental grain sizes ($d = 5-15\ \mu$m) and $\phi_c = 5\times10^{-7} - 1\times10^{-5}$ for natural grain sizes ($d = 1-10$ mm), for $\frac{D^{GB}}{D^{L}} = 16-30$.

Deviations from the prediction may be caused by a grain size distribution and second phases in a rock that can significantly change the degree of connectivity of regions with smaller melt fraction (i.e., there is a multiscale homogenization problem). Also, as discussed above, open questions exist on the effects of composition on grain boundary, lattice, and melt diffusivities.

3. Is There an Unextractable Melt Fraction?

When rocks are at temperatures and pressures at and above their solidi, do they always maintain a very small amount of melt, close to the critical melt fraction? Here I present a two-part argument for the existence of an unextractable, but connected melt distribution: (1) even if the melt fraction remains as a fully connected network, permeability will remain very low; (2) more importantly, surface tension will not allow that small melt fraction to be extracted.

1. At such small but connected melt fractions on the order of ϕ_c, isotropic permeability is very low. Using recent results of *Miller et al*. [2014], I calculate k as a function of melt fraction, using the standard expression $k = \frac{g^2\phi^n}{C}$ and their values for $n = 2.6$ and $C = 60$. The values are quite small: $k \approx 10^{-25} - 10^{-19}$, for $\phi_c = 5\times10^{-7} - 1\times10^{-5}$ at $d = 1-10$ mm, as illustrated in Figure 3b. Thus, though the critical melt fraction is by definition already forming a connected network, migration through that network will be slow.
2. Even if the melt is mobile, surface tension at the triple junction scale will resist gravitational forces that try to completely drain a very small melt fraction. At high temperature, surface tension forces have a strong influence on the melt distribution and, because they are proportional to the curvature of the melt-solid interface, they increase as the melt fraction decreases. *von Bargen and Waff* [1986] compared these potential energies (gravitational and interfacial), detailed in Appendix B and illustrated in Figures 3b and 3c. They, a length scale over which the two energy changes are balanced, here called $L_{eq.}$ (for "equivalent"). This length scale is interpreted as the vertical height of connected melt required for gravitational forces to overcome surface tension at the grain scale. Alternatively, $L_{eq.}$ is the length scale below which surface tension can homogenize the melt distribution, overcoming gravitational forces. As illustrated in Figure 3d, at $\phi_c = 10^{-6}$, $L_{eq.} = 30, 40, 50$ with 5 mm grain size, for $\theta = 10, 20, 30^{\circ}$. As ϕ decreases toward $1e-7$, $L_{eq.}$ increases quickly up to 100 km or more, on the order of the thickness of the LVZ. As discussed above (due to the same surface tension causing the melt to form connected networks), this melt fraction is likely to be connected and mobile but also, as melt fraction decreases it becomes increasingly unextractable. Thus, surface tension may provide an effective lower threshold for extractable melt. *Stevenson* [1986] and *Hier-Majumder et al*. [2006] made similar arguments.

The idea of an unextractable melt fraction is related to and consistent with the notion that the bulk viscosity approaches infinity as the melt fraction decreases, often assumed to have a form $\xi \propto \frac{1}{\phi}$. In TH2, the bulk viscosity as a function of melt fraction was found to have a different behavior, but does become much higher as $\phi < \phi_c^{\xi}$, rendering difficult the extraction of small melt fractions, in addition to the surface tension effects. Thus, kinetics (permeability), rheology (bulk viscosity), and energetics ($L_{eq.}$) all contribute to ensuring that a very small melt fraction is retained in the asthenosphere where thermodynamically possible.

4. Is This Unextractable Melt Fraction Detectable?

The significant effects of a very small melt fraction on the diffusion creep shear viscosity have implications for the detectability of an unextractable melt fraction using measurements of the seismic wavefield. Relating the long-term steady state viscosity to the short term effects of anelasticity on the propagation of a seismic wave is a large conceptual leap but has a good physical justification. The concept of a "high temperature background" (HTB) anelasticity implicates a single process that operates from the Maxwell frequency almost all the way to the purely elastic behavior. At present, a good candidate for such a process is transient grain boundary diffusion creep [e.g., *Raj*, 1975; *Cooper*, 2002a; *McCarthy et al*., 2011; *Jackson and Faul*, 2010]. Even if other processes occur in a frequency band of interest, the HTB provides reference

mechanical properties at a given thermodynamic state. For example, dislocation creep likely contributes to the total creep rate, and melt squirt or dislocation jiggling may contribute to the anelasticity at seismic frequencies, but the diffusion creep provides the reference state on which these other processes may be superimposed. A convenient term for this general idea is "Very Broadband Rheology" (VBR).

While many questions remain in constructing a robust anelastic model for the upper mantle, there is enough understanding to start constructing methods for systematic calculation and prediction of material properties (and uncertainties) across the spectrum of forcing frequencies in the Earth. From an input model of thermodynamic state, we calculate resulting elastic, viscous, and anelastic properties: unrelaxed moduli M_u, shear viscosity η, storage and loss moduli (M_1 and M_2, relaxed elastic moduli M_r, attenuation (Q^{-1}), and the isotropic shear velocity, V_s). Below and in Appendix C, I describe in more detail the calculation methods incorporating the effects of melt on each property.

4.1. Viscosity and Elasticity

Rocks at high temperature and low stress are deforming by some combination of dislocation creep, diffusion creep, and dislocation-accommodated grain boundary sliding (GBS) creep, described in more detail in Appendix C1. The temperature-melt trade-off for steady state viscosity is shown in Figure 4a. The rapid drop in viscosity with increasing melt fraction near zero at these conditions indicates that diffusion creep is contributing significantly at these conditions (with the assumptions discussed in Appendix C1). Except for $\phi \leq \phi_c$, η is much more sensitive to T than to ϕ. In elasticity, the trade-offs between the anharmonic temperature effects and the poroelastic effects on Vs are shown in Figure 4b. The sensitivity is fairly linear; the reduction in Vs of $d\phi \approx 1\%$ is equivalent to $dT \approx 150^{\circ}$.

4.2. Anelasticity

While there is consensus on transient diffusion creep being the measured HTB process in experimental samples [e.g., *Raj*, 1975; *Cooper*, 2002b; *Jackson and Faul*, 2010; *McCarthy et al*., 2011], it is possible that other dissipative processes are important in the mantle. Another possibility for the HTB mechanism is transient diffusion creep on the dislocation subgrain structure [e.g., *Gribb and Cooper*, 1998]; this hypothesis is more difficult to study in mantle silicates at the fine grain sizes necessary for experimental conditions. However, there is certainly a basis at present for proceeding with constructing estimations of the effects of melt on the anelastic properties. *McCarthy and Takei* [2011] demonstrated that the effect of very small melt fractions on viscosity also appears in the attenuation response of partially molten borneol + diphenylamine. *Gribb and Cooper* [2000] showed a modest increase (factor of 6) in attenuation values when comparing a nominally melt-free sample with one with ϕ=0.05, consistent with the exponential enhancement exp $(\alpha\phi)$. Similar to the creep experiments discussed above, it is possible that the nominally melt-free sample contains $\phi \approx \phi_c$. This speculation is based on their reporting of nonnegligible accessory phases and components. In contrast, *Jackson et al*. [2006] found a very significant effect of a small melt fraction on the measured attenuation, similar to their subsequent creep study [*Faul and Jackson*, 2007]. Thus, considering the similitude demonstrated between partially molten borneol and olivine anelasticity [*McCarthy et al*., 2011], a reasonable approach to incorporating the effect of melt into the scaling is to apply equation (1) directly to the pseudoperiod scaling in *Jackson and Faul* [2010], in the form described in *Bellis and Holtzman* [2014]. The anelastic storage and loss compliances, J_1 and J_2, are calculated for the high-temperature background attenuation (HTB) using the Andrade model with pseudoperiod scaling [*Gribb and Cooper*, 1998; *Jackson and Faul*, 2010; *Sundberg and Cooper*, 2010; *Bellis and Holtzman*, 2014], from which we calculate shear attenuation Q_s and the relaxed moduli M_r. Many open questions in this scaling problem remain [e.g., *Takei et al*., 2014]. Secondary dissipative mechanisms such as melt squirt [*Hammond and Humphreys*, 2000], elastically accommodated grain boundary sliding [e.g., *Morris and Jackson*, 2009; *Karato*, 2012], dislocation jiggling [*Farla et al*., 2012], and effects of secondary phases [e.g., *Sundberg and Cooper*, 2010] will also be explored.

When effects of melt and T are plotted together, the effect of ϕ_c appears as a rapid drop in the $T-\phi$ trade-off on a chosen V_s contour, as illustrated in Figure 4c. We calculate the difference between the unrelaxed and relaxed V_s, and plot contours of % difference in Figure 4d. The anelastic effect on V_s is increasingly significant above about 1250°C. As an example, assuming that the LAB corresponds to the solidus and the LAB temperature (equal across the LAB) of 1350°C, one could interpret the velocity contrast as measured from receiver functions or other converted phases at about 5% [e.g., *Rychert et al*., 2012; *Schmerr*, 2012], as a transition from truly melt-free to $\phi \approx 0.01$, from Figure 4c. (Note that this plot shows velocities at frequency $f = 0.01$ Hz, for

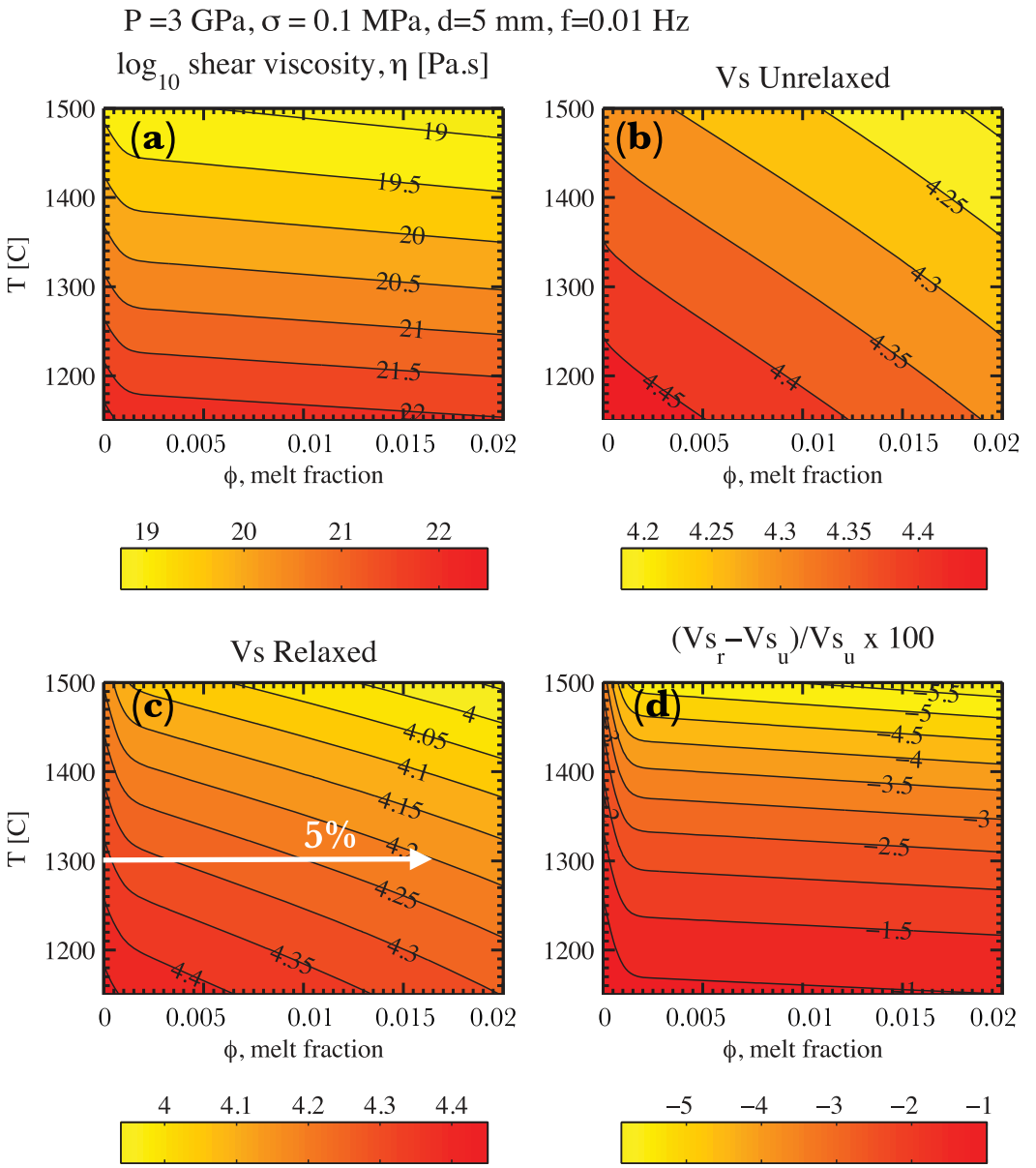

Figure 4. Trade-offs between T and ϕ on the viscous, elastic, and anelastic properties (as expressed in shear wave velocity). (a) Shear viscosity as a function of ϕ and T. (b) Unrelaxed elastic *Vs*: anharmonic thermal versus poroelastic effects on velocity. (c) Anelastic effects of T and ϕ. The arrow indicates how one could interpret the velocity contrast across an LAB at approximate thermal equilibrium. (d) The difference between relaxed and unrelaxed *Vs*, in %. The effect of small melt fraction is clear, and also the anelastic effects become increasingly significant at asthenospheric temperatures.

surface waves sensitive to the LVZ; at higher frequency, the velocities will increase slightly.) This drop in velocity across the LAB would be consistent with a decrease in shear viscosity by about a factor of 3.

4.3. Electrical Conductivity

This idea that a very small melt fraction is retained in the asthenosphere is relevant to the interpretation of electrical conductivity measurements in the Earth. Conductivity is determined by the same compositional and microstructural properties as rheological properties but with potentially very different sensitivities [e.g., *Tyburczy and du Frane*, 2015]. For example, current controversy exists on the effects of water (hydrogen) on (anisotropic) conductivity in olivine [e.g., *Wang et al.*, 2006; *Yoshino et al.*, 2009; *Yoshino and Katsura*, 2013; *Karato*, 2013; *Gardés et al.*, 2014], with significant differences in extrapolations to mantle conditions. Similarly, the effect of melt is strongly dependent on its composition [e.g., *Roberts and Tyburczy*, 1999; *Gaillard*

et al., 2008; *Tyburczy and du Frane*, 2015] and melt geometry [e.g., *Caricchi et al*., 2011; *Sifré et al*., 2014; *Pommier et al*., 2015; *Miller et al*., 2015]. It is possible that measurement of electrical conductivity may be an effective means of identifying ϕ_c and the onset of a connected melt fraction in experiments [e.g., *Tyburczy and du Frane*, 2015] and its existence in the asthenosphere.

5. Discussion and Open Questions

5.1. Are the Unextractable and Critical Melt Fractions the Same?

An obvious question is how these small melt fractions are related: Is the (mechanical) critical melt fraction physically related to the unextractable melt fraction? It is established that ϕ_c is greater than the minimum melt fraction at which melt tubules become connected (TH1,2). At $\phi \leq \phi_c$, a connected network exists that significantly weakens the long-term viscosity and increases the attenuation, affects the electrical conductivity, is a reservoir of incompatible elements, and cannot be extracted at temperatures at or above the solidus. Other microscopic thermodynamic and kinetic considerations are beyond the scope of this paper, such as the ability of surface tension to provoke dissolution [*Takei and Hier-Majumder*, 2009] and/or melting as long as there is a source of meltable components (i.e., clinopyroxene) in the vicinity (diffusion distance) of a grain edge tubule [*Hiraga and Kohlstedt*, 2009]. Surface tension will act to restore a connected melt fraction, either by driving melt advection or by driving dissolution or melting [*Takei and Hier-Majumder*, 2009]. If melt fraction rises well above ϕ_c, then it will begin to drain more quickly. If melt is locally drained to fall below the connected melt fraction, melt productivity would be "batch melting," quickly bringing ϕ back up to $\phi \approx \phi_c$ or greater. Thus, the local average melt fraction may oscillate around ϕ_c, as long as the thermodynamic conditions for melting are met.

5.2. Melt Distribution in the Asthenosphere

How do buoyancy-driven migration and surface tension-driven retention interact in a naturally heterogeneous, open system? Spatial heterogeneity in major and trace elements may be a ubiquitous property of the convecting mantle, produced by mechanical mixing of subducted plates forming fertile pyroxenites, delaminated lithosphere or other sources. Heterogeneity in major element composition (i.e., pyroxene distribution) and volatile content may exist due to a variety of reasons, and fluxes of CO_2 from deeper mantle sources may occur at time scales much shorter than the convective time scales [e.g., *Hirschmann*, 2010]. Also, the melt migration/compaction process can generate porosity waves, potentially even in regions with low background melt fractions [*Rabinowicz et al*., 2002]. These sources of complexity suggest that melt production and migration may be heterogeneous and transient in time and space, even in regions of low productivity.

When the asthenosphere is sampled by seismic waves, patchy low porosity may cause scattering or simply appear as a homogeneous volume depending on the length scale of variability and the seismic wavelength. As shown in Figure 4c, for example, if the middepth core of the oceanic low-velocity zone is at 4.1–4.2 km/s, the trade-off between temperature and melt fraction can be read by following that velocity contour. *Karato* [2012] dismissed the effect of melt on reducing V_s because he assumed that melt had to *wet the grain boundaries* in order to have significant effects and that a melt fraction sufficient to do so would not be present. While the latter point is probably true, the former is neglecting all the research that is the basis for this letter: a significant effect of melt on seismic velocity can occur due to a connected network of triple junctions at very small melt volume, *without* melt films on fully wetted grain boundaries.

As discussed in section 4.3, magnetotelluric measurements also provide independent and complementary nonmechanical constraints on volatiles and melt content, geometry, and composition. While the conductivity of the asthenosphere in the MELT region called for a significant melt fraction of $\phi \approx 0.01-0.02$ [*Evans et al*., 1999], the recent measurement in the NoMELT region by *Sarafian et al*. [2015] are consistent with dissolved water alone, or a very small melt fraction of $\phi \approx 0.0001$, also consistent with the findings of *Sifré et al*. [2014]. Furthermore, the observation that the electrical conductivity appears to be isotropic beneath the NoMELT region may also be consistent with the presence of a very small melt fraction. Although stress can align melt at the grain scale during deformation, it is unlikely that very small melt fractions would be aligned, as deviatoric stress would compete with surface tension. Because melt is much more conductive than the crystalline matrix, and a network of very small melt fraction is likely to be isotropic, the isotropy in conductivity may indicate that the melt conductivity is overwhelming that of an anisotropic solid matrix.

5.3. Melt Distribution at the LAB

This discussion of very small melt fractions is focused on regions of the asthenosphere where melt productivity is low (Figure 1a). If the large mechanical effects discussed here occur, it seems difficult to avoid that the LAB beneath the oceanic lithosphere coincides with a (volatile-fluxed) solidus. Melt that does migrate through the asthenosphere up to the LAB can have several fates. As for the depth of the LAB, the thermal structure evolution is not fully understood [e.g., *Grose*, 2012], nor is the leakiness of the LAB to melts [*Havlin et al*., 2013], nor is the volatile content of the asthenosphere, all of which will affect the thermal structure and the melt distribution at and below the LAB. In regions of high productivity (and high strain rate), it is of course possible to have significantly higher melt fractions locally or pervasively. Shear along the interface can organize and help focus melt along an LAB [e.g., *Holtzman and Kendall*, 2010], with significant velocity contrast and additional viscosity reduction [*Holtzman et al*., 2012].

This range of processes can explain the heterogeneity in sharpness and reflectivity of the LAB of 3–10% over $<$20 km [e.g., *Bagley and Revenaugh*, 2008; *Kawakatsu et al*., 2009; *Schmerr*, 2012]. For example, velocity contrasts of 5% can reflect the onset of a small melt fraction across a solidus, as discussed above and illustrated in Figure 4c; larger contrasts can reflect concentrated melt and/or organized melt structures [*Takei and Holtzman*, 2009a; *Kawakatsu et al*., 2009; *Holtzman and Kendall*, 2010], beyond those shown in Figures 4a and 4c.

6. Conclusions

I summarize results from TH1,2 on the effect of a very small melt fraction on the diffusion creep viscosity. A simple parameterization can describe these effects that can be used to analyze experimental data and also to explore potential expressions in seismic properties and geodynamic-scale models. The magnitude of these weakening effects will depend on the rock/melt composition as manifested in the relative diffusivities of melt and grain boundaries. It is unlikely that such small melt fractions could be removed from the asthenosphere; surface tension on very small melt tubules will dominate over buoyancy forces in maintaining the connected network. Even if diffusion creep is not the dominant deformation mechanism in long term creep, the effect of melt can strongly enhance the influence of transient diffusion creep in the high-temperature background anelastic properties, expressed as attenuation and relaxed velocities. Thus, it is likely that a small melt fraction will have clear seismic, and potentially magnetotelluric, signatures that could give rise to the seismically observed and geodynamically necessary asthenosphere.

Appendix A: Estimation of Tubule Size for a Given Melt Fraction

The volume of melt in a representative elementary volume defined by one grain and its melt is most simply approximated by a sphere with thin toruses fitting tightly along great circles (hoops) representing melt tubules. The melt volume can be approximately described by N_r hoops with cross-sectional area (that can be thought of as the equivalent circular area of a grain-edge triple junction cross section) of $a_{eq}=\pi r_{eq}^2$ and volume $N_r a_{eq}\pi d$. The melt fraction is the ratio of total hoop volume to total volume, or $\phi \approx \frac{N_r a_{eq}\pi d}{(\pi/6)d^3+N_r a_{eq}\pi d}$ $\approx \frac{N_r a_{eq}\pi}{(\pi/6)d^2}$ for small ϕ. Assuming the length scale of one side of a melt tubule is approximately the diameter of the equivalent circle area, $\delta_{tubule} \approx 2r_{eq}$, we rearrange for $\delta_{tubule}=\left(\frac{2d^2\phi}{3\pi N_r}\right)^{1/2}$. $N_r=4$ can be arranged such that the surface of the sphere can be subdivided into 14 faces (determined using rubber bands and a ball), approximating the tetrakaidecahedral geometry of TH1. Much more sophisticated approaches exist [e.g., *von Bargen and Waff*, 1986]. In Figure 1c, the approximate tube wall width, δ_{tubule}, is plotted as a function of melt fraction, parameterized by grain size, compared to experimental data. For a given melt fraction, a larger grain has a larger δ_{tubule} because the sphere volume rises more quickly than the tubule volume, so that must be made up by increasing the tube thickness, by volume conservation. However, in high-temperature conditions, there are other physics at play than just mass conservation; surface tension energetics promote constant mean interfacial curvature in a system and thus the form and cross-sectional area of melt tubules will be the same across a sample at textural equilibrium, regardless of grain size [e.g., *Wark and Watson*, 2000]. Thus, fine-grained rocks can contain higher melt fractions than coarse-grained rocks at textural equilibrium because they simply have more tubules of the same cross-sectional area than do coarse-grained rocks. Mass balance and surface tension can compete during grain growth, and affect local

melt pressure and distribution, causing a coexistence of small-scale tubules and grain boundary films, as observed by e.g., *Garapić et al*. [2013].

Appendix B: How Surface Tension Resists Buoyancy-Driven Melt Flow

Several workers have studied how the force of melt buoyancy is balanced by or competes with surface tension [*Waff*, 1980; *Stevenson*, 1986; *von Bargen and Waff*, 1986; *Hier-Majumder et al*., 2006]. *von Bargen and Waff* [1986] and *Waff* [1980] cast the competition between buoyancy and surface tension in terms of energetics. Here I employ the approach of *von Bargen and Waff* [1986], as it contains the most detail in the grain-scale geometry of melt. They calculate the gravitational energy change (final-initial) due to buoyant upwelling and draining of melt from a volume, ΔU_g, as

$$\Delta U_g = \frac{Agh^2}{2}\phi(\phi-1)\Delta\rho, \tag{B1}$$

where A is the horizontal area and h is the height of the column, and $\Delta\rho$ is the density difference between melt and solid ($\Delta\rho \approx 200$ kg/m^3 at asthenospheric pressures). Competing with the buoyancy, the internal change of surface energy due to the removal of a wetting melt from that same volume, ΔU_s is derived as

$$\Delta U_s = -\Delta E^v \frac{Ah\gamma_{sl}}{d} + A\gamma_{sl}, \tag{B2}$$

where ΔE^v is the normalized surface energy change associated with the removal of melt, $\Delta E^v \frac{d}{\gamma_{sl}} = b\phi^p$, and A is the cross-sectional area of the partially molten column. The constants in the RHS are fit to calculations, as $b = b_2\theta^2 + b_1\theta + b_0$ and $p = p_2\theta^2 + p_1\theta + p_0$, where θ is the wetting angle between solid and melt, with $\theta \approx 10-35^\circ$ [e.g., *Garapić et al*., 2013], and $b_0 = -2.4297, b_1 = 5.99e-3, b_2 = 4.873e-4$ and $p_0 = 0.47865, p_1 = -1.2971e-4, p_2 = 2.745e-5$ [*von Bargen and Waff*, 1986, Table 2]. This fitting function could be replaced by a function of contiguity that would be more consistent with the analysis of TH1,2, but that is beyond the scope of this paper. Setting these two energy changes equal allows them to define a critical height at which the two are equal.

$$L_{eq.} = \frac{2\Delta E^v\gamma_{sl} - \sqrt{4(\Delta E^v\gamma_{sl})^2 - 8\phi(\phi-1)g\Delta\rho d^2\gamma_{sl}}}{2\phi(\phi-1)g\Delta\rho d}. \tag{B3}$$

In Figure 3c, I plot this equation with ϕ as an independent variable, and θ as a parameter, at fixed grain size (5 mm).

Appendix C: Mechanical Properties Calculations

C1. Viscosity

Here I use the flow laws from *Hansen et al*. [2011], of the form $\dot{\varepsilon} = \sum_{i=1:3}\dot{\varepsilon}_i$ where $\dot{\varepsilon}_i = A_i\sigma^{n_i}d^{-p_i}f_i(\phi)\exp(-Q_i/RT)$, i represents the three creep mechanisms acting in series and their respective constants, and $f_i(\phi)$ is that discussed in sections 2.3 and 2.4. For diffusion creep, I use $x_{\phi_c} = 5$, assuming that only the geometric effect is at play when a rock crosses its solidus but does not change bulk composition. For dislocation- and GBS-creep, I assume that $x_{\phi_c} = 1$ ($c_1 = 0$), though this needs further study. In this paper I set these to 1 to simplify the calculations for low melt fraction and focus on the effects on diffusion creep. To make Figure 2, I selected data from *Faul and Jackson* [2007, hereinafter FJ07] and *Hirth and Kohlstedt* [1995a, hereinafter HK95] experiments that were well into the diffusion creep regime, at low stresses far from the transition, and scaled (s) the measured data (m) as follows:

$$\dot{\varepsilon}_s = \dot{\varepsilon}_m\left(\frac{d_s}{d_m}\right)^{-p}\left(\frac{\sigma_s}{\sigma_m}\right)^{n}\left(\exp\left(\frac{-E}{RT_s} + \frac{E}{RT_m}\right)\right). \tag{C1}$$

For HK95 data, I used $n = 1$, $p = 3.2$, and $E = 575$ kJ/mol; for FJ07 data, I used $n = 1.4$, $p = 3$, and $E = 484$ kJ/mol, and normalized all points by the highest viscosity value from FJ07.

C2. Elasticity

For the unrelaxed elastic properties, the anharmonic effects of temperature and pressure are calculated using the partial derivatives $\partial M_u/\partial T = -13.6$ [MPa/K] and $\partial M_u/\partial P = 1.8$ [Pa/Pa], and a reference value

M_u^0=65.0 GPa, as in *Jackson and Faul* [2010] and *Isaak* [1992]. The effect of melt on the purely elastic properties is caused by low-modulus inclusions embedded in a matrix, referred to as the "poroelastic" effect [e.g., *O'Connell and Budiansky*, 1977; *Hammond and Humphreys*, 2000]. The poroelastic effect is calculated using the contiguity model, with the method in *Takei* [2002, Appendix A], a parameterization of the isotropic solutions of *Takei* [1998]. Comparison of predictions from other approaches [e.g., *Hier-Majumder and Abbott*, 2010] will be included in future work.

Acknowledgments
I would like to thank Takehiko Hiraga, David Kohlstedt, Christine McCarthy, Christopher Havlin, Andrea Tommasi, Leïla Hashim, and especially Yasuko Takei, who generously and critically scrutinized this paper. As I hope is clear, the core of the paper (section 2) is based on ideas developed in *Takei and Holtzman* [2009b]. This work was funded by NSF EarthScope grant EAR-0952202 and NSF Geophysics CAREER grant EAR-1056332. LDEO contribution 7964.

References

Anderson, D., and C. Sammis (1970), Partial melting in the upper mantle, *Phys. Earth Planet. Inter.*, *3*, 41–50, doi:10.1016/0031-9201(70)90042-7.
Bagley, B., and J. Revenaugh (2008), Upper mantle seismic shear discontinuities of the pacific, *J. Geophys. Res.*, *113*, B12301, doi:10.1029/2008JB005692.
Bellis, C., and B. Holtzman (2014), Sensitivity of seismic measurements to frequency-dependent attenuation and upper mantle structure: An initial approach, *J. Geophys. Res. Solid Earth*, *119*, 5497–5517, doi:10.1002/2013JB010831.
Braun, M., G. Hirth, and E. Parmentier (2000), The effects of deep damp melting on mantle flow and melt generation beneath mid-ocean ridges, *Earth Planet. Sci. Lett.*, *176*(3–4), 339–356.
Caricchi, L., F. Gaillard, J. Mecklenburgh, and E. Le Trong (2011), Experimental determination of electrical conductivity during deformation of melt-bearing olivine aggregates: Implications for electrical anisotropy in the oceanic low velocity zone, *Earth Planet. Sci. Lett.*, *302*(1), 81–94.
Cooper, R., and D. Kohlstedt (1986), Rheology and structure of olivine-basalt partial melts, *J. Geophys. Res.*, *91*(B9), 9315–9323.
Cooper, R. F. (2002), Seismic wave attenuation: Energy dissipation in viscoelastic crystalline solids, *Rev. Mineral. Geochem.*, *51*(1), 253–290.
Dasgupta, R., M. M. Hirschmann, and N. D. Smith (2007), Water follows carbon: CO_2 incites deep silicate melting and dehydration beneath mid-ocean ridges, *Geology*, *35*(2), 135–138.
Eggler, D. H. (1976), Does CO_2 cause partial melting in the low-velocity layer of the mantle?, *Geology*, *4*, 69–72, doi:10.1130/0091-7613(1976)4¡69:DCCPMI¿2.0.CO;2.
Evans, R., et al. (1999), Asymmetric electrical structure in the mantle beneath the east pacific rise at 17 s, *Science*, *286*(5440), 752–756.
Farla, R. J., I. Jackson, J. D. F. Gerald, U. H. Faul, and M. E. Zimmerman (2012), Dislocation damping and anisotropic seismic wave attenuation in earth's upper mantle, *Science*, *336*(6079), 332–335.
Faul, U., and I. Jackson (2007), Diffusion creep of dry, melt-free olivine, *J. Geophys. Res.*, *112*, B04204, doi:10.1029/2006JB004586.
Faul, U. H., F. Gerald, D. John, and I. Jackson (2004), Shear wave attenuation and dispersion in melt-bearing olivine polycrystals: 2. Microstructural interpretation and seismological implications, *J. Geophys. Res.*, *109*, B06202, doi:10.1029/2003JB002407.
Gaillard, F., M. Malki, G. Iacono-Marziano, M. Pichavant, and B. Scaillet (2008), Carbonatite melts and electrical conductivity in the asthenosphere, *Science*, *322*(5906), 1363–1365.
Garapić, G., U. Faul, and E. Brisson (2013), High-resolution imaging of the melt distribution in partially molten upper mantle rocks: Evidence for wetted two-grain boundaries, *Geochem. Geophys. Geosyst.*, *14*, 556–566, doi:10.1029/2012GC004547.
Gardés, E., F. Gaillard, and P. Tarits (2014), Toward a unified hydrous olivine electrical conductivity law, *Geochem. Geophys. Geosyst.*, *15*, 4984–5000, doi:10.1002/2014GC005496.
Green, D. H., and R. C. Liebermann (1976), Phase equilibria and elastic properties of a pyrolite model for the oceanic upper mantle, *Tectonophysics*, *32*, 61–92.
Gribb, T., and R. Cooper (1998), Low-frequency shear attenuation in polycrystalline olivine: Grain boundary diffusion and the physical significance of the Andrade model for viscoelastic rheology, *J. Geophys. Res.*, *103*(B11), 27,267–27,279.
Gribb, T., and R. Cooper (2000), The effect of an equilibrated melt phase on the shear creep and attenuation behavior of polycrystalline olivine, *Geophys. Res. Lett.*, *27*(15), 2341–2344.
Grose, C. J. (2012), Properties of oceanic lithosphere: Revised plate cooling model predictions, *Earth Planet. Sci. Lett.*, *333*, 250–264.
Hammond, W., and E. Humphreys (2000), Upper mantle seismic wave attenuation: Effects of realistic partial melt distribution, *J. Geophys. Res.*, *105*(B5), 10,987–10,999.
Hansen, L. N., M. E. Zimmerman, and D. L. Kohlstedt (2011), Grain boundary sliding in San Carlos olivine: Flow law parameters and crystallographic-preferred orientation, *J. Geophys. Res.*, *116*, B08201, doi:10.1029/2011JB008220.
Havlin, C., E. Parmentier, and G. Hirth (2013), Dike propagation driven by melt accumulation at the lithosphere–asthenosphere boundary, *Earth Planet. Sci. Lett.*, *376*, 20–28.
Hier-Majumder, S., and M. E. Abbott (2010), Influence of dihedral angle on the seismic velocities in partially molten rocks, *Earth Planet. Sci. Lett.*, *299*(1), 23–32.
Hier-Majumder, S., Y. Ricard, and D. Bercovici (2006), Role of grain boundaries in magma migration and storage, *Earth Planet. Sci. Lett.*, *248*(3–4), 735–749, doi:10.1016/j.epsl.2006.06.015.
Hiraga, T., and D. L. Kohlstedt (2007), Equilibrium interface segregation in the diopside–forsterite system I: Analytical techniques, thermodynamics, and segregation characteristics, *Geochim. Cosmochim. Acta*, *71*(5), 1266–1280.
Hiraga, T., and D. L. Kohlstedt (2009), Systematic distribution of incompatible elements in mantle peridotite: Importance of intra-and intergranular melt-like components, *Contrib. Mineral. Petrol.*, *158*(2), 149–167.
Hiraga, T., M. M. Hirschmann, and D. L. Kohlstedt (2007), Equilibrium interface segregation in the diopside–forsterite system II: Applications of interface enrichment to mantle geochemistry, *Geochim. Cosmochim. Acta*, *71*(5), 1281–1289.
Hirschmann, M. M. (2010), Partial melt in the oceanic low velocity zone, *Phys. Earth Planet. Inter.*, *179*(1), 60–71.
Hirth, G., and D. L. Kohlstedt (1995a), Experimental constraints on the dynamics of the partially molten upper mantle: Deformation in the diffusion creep regime, *J. Geophys. Res.*, *100*(B2), 1981–2001.
Hirth, G., and D. L. Kohlstedt (1995b), Experimental constraints on the dynamics of the partially molten upper mantle 2. Deformation in the dislocation creep regime, *J. Geophys. Res.*, *100*(B8), 15,441–15,449.
Hirth, G., and D. L. Kohlstedt (1996), Water in the oceanic upper mantle: Implications for rheology, melt extraction and the evolution of the lithosphere, *Earth Planet. Sci. Lett.*, *144*(1), 93–108.
Hirth, G., and D. L. Kohlstedt (2003), Rheology of the upper mantle and the mantle wedge: A view from the experimentalists, in *Inside the Subduction Factory*, edited by J. Eiler, pp. 83–105, AGU, Washington, D. C.

Holtzman, B. K., and J.-M. Kendall (2010), Organized melt, seismic anisotropy, and plate boundary lubrication, *Geochem. Geophys. Geosyst.*, *11*, Q0AB06, doi:10.1029/2010GC003296.
Holtzman, B. K., D. S. King, and D. L. Kohlstedt (2012), Effects of stress-driven melt segregation on the viscosity of rocks, *Earth Planet. Sci. Lett.*, *359*, 184–193.
Isaak, D. G. (1992), High-temperature elasticity of iron-bearing olivines, *J. Geophys. Res.*, *97*(B2), 1871–1885.
Jackson, I., and U. H. Faul (2010), Grainsize-sensitive viscoelastic relaxation in olivine: Towards a robust laboratory-based model for seismological application, *Phys. Earth Planet. Inter.*, *183*(1–2), 151–163.
Jackson, I., U. Faul, J. Fitzgerald, and S. Morris (2006), Contrasting viscoelastic behavior of melt-free and melt-bearing olivine: Implications for the nature of grain-boundary sliding, *Mater. Sci. Eng. A*, *442*(1–2), 170–174, doi:10.1016/j.msea.2006.01.136.
Karato, S.-I. (2012), On the origin of the asthenosphere, *Earth Planet. Sci. Lett.*, *321*, 95–103.
Karato, S.-I. (2013), Theory of isotope diffusion in a material with multiple species and its implications for hydrogen-enhanced electrical conductivity in olivine, *Phys. Earth Planet. Inter.*, *219*, 49–54.
Karato, S., and H. Jung (1998), Water, partial melting and the origin of the seismic low velocity and high attenuation zone in the upper mantle, *Earth Planet. Sci. Lett.*, *157*(3–4), 193–207.
Kawakatsu, H., P. Kumar, Y. Takei, M. Shinohara, T. Kanazawa, E. Araki, and K. Suyehiro (2009), Seismic evidence for sharp lithosphere-asthenosphere boundaries of oceanic plates, *Science*, *324*(5926), 499–502.
Lehner, F. K. (1995), A model for intergranular pressure solution in open systems, *Tectonophysics*, *245*(3), 153–170.
McCarthy, C., and Y. Takei (2011), Anelasticity and viscosity of partially molten rock analogue: Toward seismic detection of small quantities of melt, *Geophys. Res. Lett.*, *38*, L18306, doi:10.1029/2011GL048776.
McCarthy, C., Y. Takei, and T. Hiraga (2011), Experimental study of attenuation and dispersion over a broad frequency range: 2. The universal scaling of polycrystalline materials, *J. Geophys. Res.*, *116*, B09207, doi:10.1029/2011JB008384.
Mei, S., W. Bai, T. Hiraga, and D. Kohlstedt (2002), Influence of melt on the creep behavior of olivine-basalt aggregates under hydrous conditions, *Earth Planet. Sci. Lett.*, *201*(3–4), 491–507, doi:10.1016/S0012-821X(02)00745-8.
Miller, K. J., W.-L. Zhu, L. G. Montési, and G. A. Gaetani (2014), Experimental quantification of permeability of partially molten mantle rock, *Earth Planet. Sci. Lett.*, *388*, 273–282.
Miller, K. J., L. G. Montési, and W.-L. Zhu (2015), Estimates of olivine–basaltic melt electrical conductivity using a digital rock physics approach, *Earth Planet. Sci. Lett.*, *432*, 332–341.
Minarik, W. G., and E. B. Watson (1995), Interconnectivity of carbonate melt at low melt fraction, *Earth Planet. Sci. Lett.*, *133*(3), 423–437.
Morris, S., and I. Jackson (2009), Diffusionally assisted grain-boundary sliding and viscoelasticity of polycrystals, *J. Mech. Phys. Solids*, *57*(4), 744–761.
O'Connell, R., and B. Budiansky (1977), Viscoelastic properties of fluid-saturated cracked solids, *J. Geophys. Res.*, *82*(36), 5719–5735.
Phipps Morgan, J. (1997), The generation of a compositional lithosphere by mid-ocean ridge melting and its effect on subsequent off-axis hotspot upwelling and melting, *Earth Planet. Sci. Lett.*, *146*(1), 213–232.
Pommier, A., K. Leinenweber, D. L. Kohlstedt, C. Qi, E. J. Garnero, S. J. Mackwell, and J. A. Tyburczy (2015), Experimental constraints on the electrical anisotropy of the lithosphere-asthenosphere system, *Nature*, *522*(7555), 202–206.
Rabinowicz, M., Y. Ricard, and M. Grégoire (2002), Compaction in a mantle with a very small melt concentration: Implications for the generation of carbonatitic and carbonate-bearing high alkaline mafic melt impregnations, *Earth Planet. Sci. Lett.*, *203*(1), 205–220.
Raj, R. (1975), Transient behavior of diffusion-induced creep and creep rupture, *Metall. Trans. A*, *6A*, 1499–1509.
Renner, J., B. Evans, and G. Hirth (2000), On the rheologically critical melt fraction, *Earth Planet. Sci. Lett.*, *181*(4), 585–594, doi:10.1016/S0012-821X(00)00222-3.
Roberts, J. J., and J. A. Tyburczy (1999), Partial-melt electrical conductivity: Influence of melt composition, *J. Geophys. Res.*, *104*(B4), 7055–7065.
Rychert, C. A., N. Schmerr, and N. Harmon (2012), The pacific lithosphere-asthenosphere boundary: Seismic imaging and anisotropic constraints from SS waveforms, *Geochem. Geophys. Geosyst.*, *13*, Q0AK10, doi:10.1029/2012GC004194.
Sarafian, E., R. L. Evans, J. Collins, J. Elsenbeck, G. Gaetani, J. B. Gaherty, G. Hirth, and D. Lizarralde (2015), The electrical structure of the central Pacific upper mantle constrained by the NoMelt experiment, *Geochem. Geophys. Geosyst.*, *16*, 1115–1132, doi:10.1002/2014GC005709.
Schmerr, N. (2012), The gutenberg discontinuity: Melt at the lithosphere-asthenosphere boundary, *Science*, *335*(6075), 1480–1483.
Scott, T., and D. Kohlstedt (2006), The effect of large melt fraction on the deformation behavior of peridotite, *Earth Planet. Sci. Lett.*, *246*(3–4), 177–187, doi:10.1016/j.epsl.2006.04.027.
Sifré, D., E. Gardés, M. Massuyeau, L. Hashim, S. Hier-Majumder, and F. Gaillard (2014), Electrical conductivity during incipient melting in the oceanic low-velocity zone, *Nature*, *509*(7498), 81–85.
Stevenson, D. (1986), On the role of surface tension in the migration of melts and fluids, *Geophys. Res. Lett.*, *13*(11), 1149–1152.
Sundberg, M., and R. F. Cooper (2010), A composite viscoelastic model for incorporating grain boundary sliding and transient diffusion creep; correlating creep and attenuation responses for materials with a fine grain size, *Philos. Mag.*, *90*(20), 2817–2840.
Takei, Y. (1998), Constitutive mechanical relations of solid-liquid composites in terms of grain-boundary contiguity, *J. Geophys. Res.*, *103*(B8), 18,183–18,203.
Takei, Y. (2002), Effect of pore geometry on Vp/Vs: From equilibrium geometry to crack, *J. Geophys. Res.*, *107*(B2), 2043, doi:10.1029/2001JB000522.
Takei, Y., and S. Hier-Majumder (2009), A generalized formulation of interfacial tension driven fluid migration with dissolution/precipitation, *Earth Planet. Sci. Lett.*, *288*(1–2), 138–148, doi:10.1016/j.epsl.2009.09.016.
Takei, Y., and B. K. Holtzman (2009a), Viscous constitutive relations of solid-liquid composites in terms of grain boundary contiguity: 1. Grain boundary diffusion control model, *J. Geophys. Res.*, *114*, B06205, doi:10.1029/2008JB005850.
Takei, Y., and B. K. Holtzman (2009b), Viscous constitutive relations of solid-liquid composites in terms of grain boundary contiguity: 2. Compositional model for small melt fractions, *J. Geophys. Res.*, *114*, B06205, doi:10.1029/2008JB005851.
Takei, Y., and B. K. Holtzman (2009c), Viscous constitutive relations of solid-liquid composites in terms of grain boundary contiguity: 3. Causes and consequences of viscous anisotropy, *J. Geophys. Res.*, *114*, B06207, doi:10.1029/2008JB005852.
Takei, Y., F. Karasawa, and H. Yamauchi (2014), Temperature, grain size, and chemical controls on polycrystal anelasticity over a broad frequency range extending into the seismic range, *J. Geophys. Res. Solid Earth*, *119*, 5414–5443, doi:10.1002/2014JB011146.
Tyburczy, J. A., and W. L. du Frane (2015), Properties of rocks and minerals—The electrical conductivity of rocks, minerals, and the earth, in *Treatise on Geophysics*, 2nd ed., pp. 661–672, Elsevier, Amsterdam.
von Bargen, N., and H. S. Waff (1986), Permeabilities, interfacial areas and curvatures of partially molten systems: Results of numerical computations of equilibrium microstructures, *J. Geophys. Res.*, *91*(B9), 9261–9276.

Waff, H. S. (1980), Effects of the gravitational field on liquid distribution in partial melts within the upper mantle, *J. Geophys. Res.*, *85*(B4), 1815–1825.
Wang, D., M. Mookherjee, Y. Xu, and S.-I. Karato (2006), The effect of water on the electrical conductivity of olivine, *Nature*, *443*(7114), 977–980.
Wark, D. A., and E. B. Watson (2000), Effect of grain size on the distribution and transport of deep-seated fluids and melts, *Geophys. Res. Lett.*, *27*(14), 2029–2032.
Yoshino, T., and T. Katsura (2013), Electrical conductivity of mantle minerals: Role of water in conductivity anomalies, *Annu. Rev. Earth Planet. Sci.*, *41*, 605–628.
Yoshino, T., T. Matsuzaki, A. Shatskiy, and T. Katsura (2009), The effect of water on the electrical conductivity of olivine aggregates and its implications for the electrical structure of the upper mantle, *Earth Planet. Sci. Lett.*, *288*(1), 291–300.
Zhu, W., G. A. Gaetani, F. Fusseis, L. G. Montési, and F. De Carlo (2011), Microtomography of partially molten rocks: Three-dimensional melt distribution in mantle peridotite, *Science*, *332*(6025), 88–91.
Zimmerman, M., and D. Kohlstedt (2004), Rheological properties of partially molten lherzolite, *J. Petrol.*, *45*(2), 275–298.

Erratum

In the originally published version of this article, a figure caption and equation were incorrect. The following have since been corrected and this version may be considered the authoritative version of record.

In Figure 1d caption, grain size was changed to grain boundary.

Figure 2 caption was changed from (a) Four curves of the parameterization, for values $\phi_c = 0.0005$, $\phi_c = 0.001$, $x^1_{\phi_c} = 5$, $x^2_{\phi_c} = 20$, $x^3_{\phi_c} = 120$ to (a) Four curves of the parameterization, for values $\phi_c = 0.0005$ *and* $\phi_c = 0.001$, $x_{\phi_c} = 5,\ 20,\ 120$.

In section 3, the sentence, "When rocks are at temperatures and pressures above their solidi, do they always maintain a very small amount of melt, close to the critical melt fraction?" was changed to "When rocks are at temperatures and pressures at and above their solidi, do they always maintain a very small amount of melt, close to the critical melt fraction?"

In section 4.1, the sentence, "Rocks at high temperature and low stress are deforming by some combination of dislocation creep and diffusion and dislocation-accommodated grain boundary sliding (GBS) creep" was changed to "Rocks at high temperature and low stress are deforming by some combination of dislocation creep, diffusion creep and dislocation-accommodated grain boundary sliding (GBS) creep".

In Appendix A, $\delta_{tubule} = \frac{2d^2\phi}{3\pi N_r}$ was changed to $\delta_{tubule} = \left(\frac{2d^2\phi}{3\pi N_r}\right)^{1/2}$.